Asian Journal of Chemistry; Vol. 36, No. 10 (2024), 2391-2396

ASIAN JOURNAL OF CHEMISTRY

https://doi.org/10.14233/ajchem.2024.32340

Synthesis of Copper-Doped Metal Nanoferrites for Efficient Removal of Pharmaceutical Wastewater Pollutants in Membrane Bioreactor System

V. NITHYA* and B. CHIRSABESAN

Department of Chemical Engineering, Annamalai University, Annamalai Nagar-608002, India

*Corresponding author: E-mail: nithyavenkt123@gmail.com

Received: 19 July 2024; *Accepted*: 10 September 2024; *Published online*: 30 September 2024; AJC-21770

Pharmaceuticals present in the aquatic environment can poison aquatic species and humans through drinking water and cause harmful bacteria to become resistant. The role of transition metal doped metal nanoferrites for the enhanced efficiency of degradation process is widely achieved. In this work, copper doped magnesium ferrite (Cu-$MgFe_2O_4$) and copper doped zinc ferrite (Cu-$ZnFe_2O_4$) nanoparticles were synthesized using a sol-gel method. X-ray diffraction (XRD) analysis confirmed the formation of the spinel structure for both samples, with crystal sizes of 16.72 nm and 59.05 nm, respectively. The magnetic properties of the samples were studied using a vibrating sample magnetometer (VSM), which revealed that the addition of Cu^{2+} ions has a significant impact on the magnetic properties of the nanoparticles. The saturation magnetisation (M_s), retentivity (M_r) and coercivity value (H_c) for the Cu-$MgFe_2O_4$ sample were found to be 0.18453 emu, 39.584×10^{-3} emu and 139.61 Oe, respectively, while for the Cu-$ZnFe_2O_4$ sample, the values were 0.21271 emu, 71.022×10^{-3} emu and 285.91 Oe, respectively. The impact of copper doped nanoferrites on pollutant removal from pharmaceutical wastewater using the membrane Bioreactor (MBR) system has also been accomplished. The results demonstrated the effectiveness of ferrites in reducing concentrations of heavy metals, including lead and cadmium, within acceptable ranges for inland surface water and public sewers. Furthermore, the MBR system with ferrites exhibited efficient removal of fluoride, sulphide and radioactivity, ensuring compliance with the specified standards. Although the study exhibited the potential of ferrites in pollutants removal, further optimization is necessary to achieve complete compliance with water quality standards.

Keywords: Copper, Nanoferrites, Pharmaceutical pollutants, Membrane bioreactor, Structural features.

INTRODUCTION

Nanotechnology in ferrites involves the creation of ferrite nanoparticles with unique magnetic and electrical properties by controlling their size, shape and composition at the nano scale level [1-4]. These nanoparticles have potential applications in a range of fields including medicine, electronics and energy [5-8]. Metal doped ferrite (MFe_2O_4) where M represents a metal ion, belongs to a class of ferrite materials that have a cubic crystal structure and are composed of transition metal oxides, such as iron oxide, cobalt oxide and nickel oxide and metal ions such as copper, nickel, zinc, cobalt or manganese [9-13].

There are several methods for synthesizing spinel ferrites, including solid-state reaction, sol-gel method, co-precipitation and hydrothermal synthesis [14-17]. The choice of synthesis method mainly depends on the desired properties and applications of the effective ferrite material. In solid-state reactions, the ferrite material is synthesized by mixing the starting materials, typically metal oxides or carbonates in the desired stoichiometric ratios and heating them at high temperatures in a controlled atmosphere [18-20]. This method is relatively simple but can result in non-uniform and impure ferrite materials. In sol-gel method, the ferrite material is synthesized by mixing metal alkoxides or salts with a solvent, such as ethanol or water, to obtain a sol, which was then dried and calcined to form the ferrite material [21-23]. This method allows for better control over the composition and morphology of the ferrite material but can be more time-consuming and expensive as compared to solid-state reactions [24].

Copper doped magnesium ferrite (Cu-Mg ferrite) and zinc doped magnesium ferrite (Zn-Mg ferrite) nanoparticles are two examples of ferrite nanoparticles that have been extensively studied for their unique properties and potential applications

in various fields [25,26]. Cu-Mg ferrite nanoparticles are synthesized by doping magnesium ferrite with copper ions [27-29], resulting in enhanced magnetic moment and coercivity, thereby rendering them advantageous for applications in magnetic data storage and biomedical fields, including magnetic hyperthermia for cancer treatment [2,30]. On the other hand, Zn-Mg ferrite nanoparticles have a high dielectric constant and low loss, making them useful for applications in electronic devices such as capacitors and microwave filters [31-35]. Both Cu-Mg and Zn-Mg ferrite nanoparticles can be synthesized using various methods, including co-precipitation, sol-gel and hydrothermal methods [15,16]. The properties and applications of these nanoparticles can be tailored by adjusting the doping concentration, particle size and shape [36-38].

This work investigate the role of the magnetic and electric properties of copper doped magnesium ferrite (Cu-$MgFe_2O_4$) and copper doped zinc ferrite (Cu-$ZnFe_2O_4$) nanoparticles and its applications in the membrane bioreactor system in pharmaceutical wastewater purification. Furthermore, the effect of copper doping on the structural, electrical and magnetic properties of these nanoferrite were also carried out.

EXPERIMENTAL

As precursor materials, magnesium nitrate hexahydrate ($Mg(NO_3)_2{\cdot}6H_2O$), copper nitrate trihydrate ($Cu(NO_3)_2{\cdot}3H_2O$), zinc nitrate hexahydrate ($Zn(NO_3)_2{\cdot}6H_2O$) and iron nitrate nonahydrate ($Fe(NO_3)_3{\cdot}H_2O$) were employed. For the capping agent and precipitate purposes in the preparation of ferrite nanoparticles, polyvinyl pyrrolidine (PVP), sodium hydroxide (NaOH), and deionized (DI) water were utilized.

Synthesis: Magnesium nitrate hexahydrate/zinc nitrate hexahydrate dissolved in 20 mL of distilled water was added of copper nitrate trihydrate solution while stirring. Then iron nitrate nonahydrate dissolved in 20 mL of distilled water in a separate beaker and then mixed to the solution solution while stirring for 30 min. By adding dropwise NaOH solution and PVP (0.2 g) as surface stabilizer while stirring the solution for 2 h to ensure the thorough mixing. Transferred the solution to a clean glass Petri dish and heat at 120 ºC for 6 h to obtain a gel. Grind the gel into a fine powder and annealed at 700 ºC for 2 h in air to form the desired nanoparticles.

RESULTS AND DISCUSSION

XRD studies: The Cu-$MgFe_2O_4$ and Cu-$ZnFe_2O_4$ nanoferrites showed a diffraction peak at 2θ is 35.56º and 35.51º, which corresponds to the (311) plane of the spinel structure (Fig. 1). The calculated crystal size of the Cu-$MgFe_2O_4$ nanoferrites using Scherrer's equation was found to be 16.72 nm. However, the calculated crystal size of Cu-$ZnFe_2O_4$ nanoferrites was found to be larger, at 59.05 nm. The JCPDS card no. for the spinel structures of copper doped magnesium ferrite and copper doped zinc ferrite are 39-1346 and 22-1086, respectively. The small difference in 2θ values between the two samples suggests that the crystal structures of these two materials are similar. However, the difference in crystal size suggests that the doping elements may have different effects on the crystal growth of the nanoferrites. Overall, these XRD results provide important information on the crystal structure and size of the copper doped magnesium ferrite and zinc doped magnesium ferrite nanoparticles, which can be used to tailor their properties for various applications.

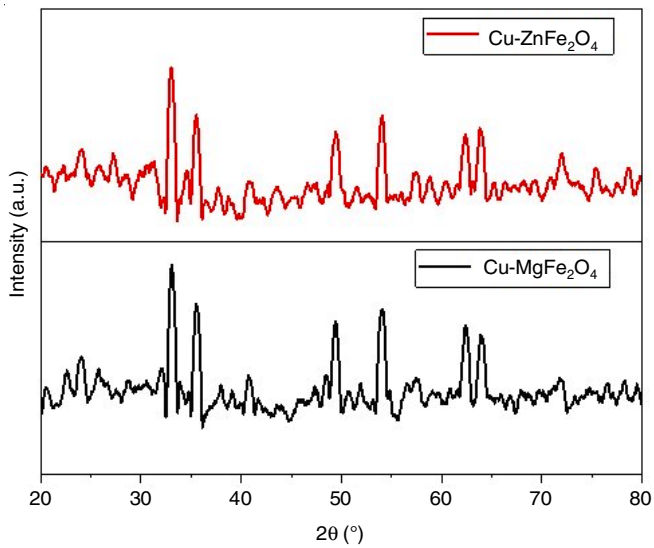

Fig. 1. XRD patterns of Cu-$MgFe_2O_4$ and Cu-$ZnFe_2O_4$ nanoferrites

FTIR studies: The FTIR spectra of Cu-$MgFe_2O_4$ and Cu-$ZnFe_2O_4$ nanoferrites are shown in Fig. 2. The peaks in the spectra correspond to the different vibrations of chemical bonds in the materials. For Cu-$MgFe_2O_4$, the peaks observed at 3434 cm^{-1} and 2924.39 cm^{-1} correspond to the stretching vibrations of O-H and C-H bonds, respectively. The peak observed at 2095.01 cm^{-1} is assigned to the stretching vibrations of Cu-O bonds, while the peak observed at 2025.99 cm^{-1} corresponds to the stretching vibrations of Mg-O bonds. The peak observed at 1631.18 cm^{-1} is assigned to the bending vibrations of H-O-H bonds. The peak observed at 1508.29 cm^{-1} corresponds to the stretching vibrations of Fe-O bonds, while the peak observed at 1406.02 cm^{-1} is assigned to the bending vibrations of Fe-O bonds. The peak observed at 1270 cm^{-1} corresponds to the stret-

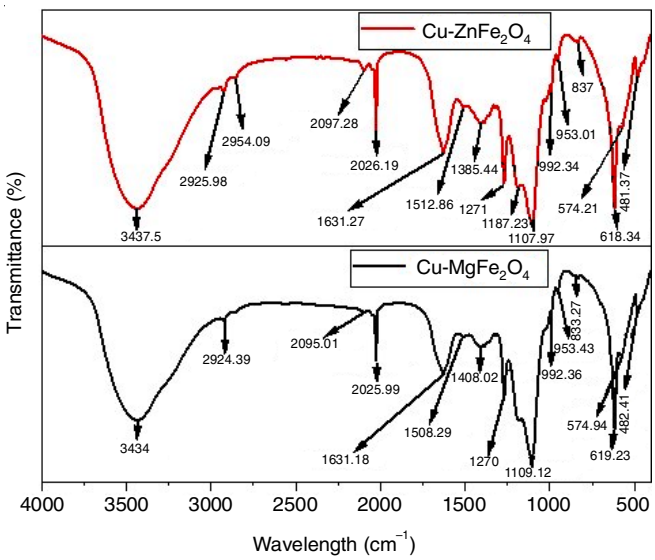

Fig. 2. FTIR spectra of Cu-$MgFe_2O_4$ and Cu-$ZnFe_2O_4$ nanoferrites

ching vibrations of Mg-O bonds, while the peak observed at 1109.12 cm^{-1} corresponds to the stretching vibrations of Fe-O bonds. The peaks observed at 992.36 cm^{-1} and 953.43 cm^{-1} correspond to the stretching vibrations of Cu-O bonds. The peak observed at 833.27 cm^{-1} corresponds to the bending vibrations of Mg-O bonds, while the peaks observed at 619.23 cm^{-1}, 574.94 cm^{-1} and 482.49 cm^{-1} correspond to the bending vibrations of Fe-O bonds.

For Cu-$ZnFe_2O_4$, the peaks observed at 3437.5 cm^{-1} and 2925.98 cm^{-1} correspond to the stretching vibrations of O-H and C-H bonds, respectively. The peak observed at 2954.09 cm^{-1} corresponds to the stretching vibrations of Zn-H bonds, while the peak observed at 2097.28 cm^{-1} is assigned to the stretching vibrations of Cu-O bonds. The peak observed at 2026.19 cm^{-1} corresponds to the stretching vibrations of Zn-O bonds, while the peak observed at 1631.27 cm^{-1} is assigned to the bending vibrations of H-O-H bonds. The peak observed at 1512.86 cm^{-1} corresponds to the stretching vibrations of Fe-O bonds, while the peak observed at 1385.44 cm^{-1} corresponds to the bending vibrations of Zn-O bonds. The peak observed at 1271 cm^{-1} corresponds to the stretching vibrations of Zn-O bonds, while the peak observed at 1187.23 cm^{-1} corresponds to the stretching vibrations of Fe-O bonds. The peak observed at 1107.97 cm^{-1} corresponds to the stretching vibrations of Cu-O bonds, while the peak observed at 992.34 cm^{-1} corresponds to the stretching vibrations of Zn-O bonds. The peak observed at 953.01 cm^{-1} corresponds to the stretching vibrations of Cu-O bonds, while the peak observed at 837 cm^{-1} corresponds to the bending vibrations of Zn-O bonds. The peaks observed at 618.34 cm^{-1}, 574.21 cm^{-1}, and 481.37 cm^{-1} correspond to the bending vibrations of Fe-O bonds.

Optical studies: The UV measurements for the copper doped magnesium ferrite and copper-doped zinc ferrite nanoparticles were performed to investigate their optical properties. In Fig. 3, the UV spectra showed a characteristic peak for each material, with a peak at 286 nm for copper doped magnesium nanoferrite and a peak at 279 nm for copper doped zinc nanoferrite. The observed peaks are related to the electronic transitions in the materials, which are influenced by the crystal structure and the presence of copper ions.

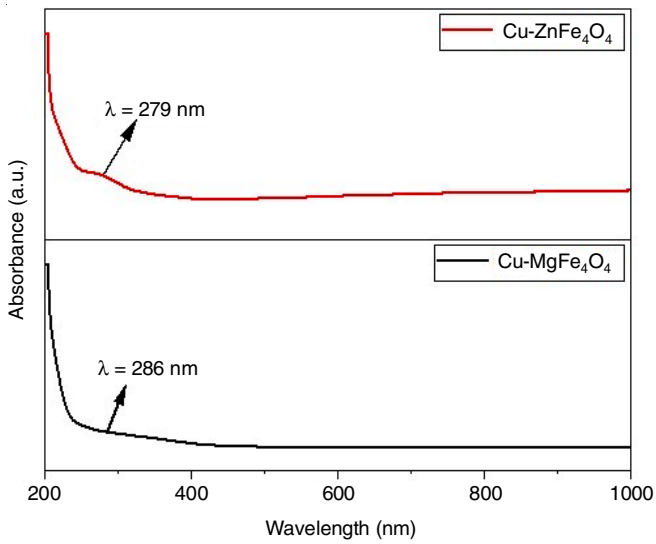

Fig. 3. UV spectra of Cu-$MgFe_2O_4$ and Cu-$ZnFe_2O_4$ nanoferrites

The observed peak at 286 nm for copper doped magnesium nanoferrite is in agreement with previous studies, which have reported peaks in the range of 250-300 nm for copper doped nanoferrites. The peak is related to the electron transitions between the occupied 3*d* and the unoccupied 4*s* states of the copper ions, which are located in the tetrahedral sites of the spinel structure. The presence of copper ions in the structure also affects the absorption edge of the material, shifting it towards the visible region and resulting in increased absorption of light in the blue-green part of the spectrum. Similarly, the peak at 279 nm for copper doped zinc nanoferrite can be attributed to the electronic transitions between the occupied 3*d* and the unoccupied 4*s* states of the copper ions, which are located in the octahedral sites of the spinel structure. The peak is consistent with previous reports of copper-doped zinc ferrites, which have shown absorption peaks in the range of 250-300 nm. Overall, the UV analysis confirmed the successful synthesis of copper doped metal ferrite nanoparticles *via* the sol-gel method, and provide insight into their electronic transitions and optical properties.

Vibrating sample magnetometer analysis: Fig. 4 displays the magnetic hysteresis loop for the prepared samples and the results show that the addition of Cu^{2+} ions into the $MgFe_2O_4$ and $ZnFe_2O_4$ nanoferrites has a significant impact on their magnetic properties. For $MgFe_2O_4$ sample, the saturation magnetization (M_s) was found to be 0.18453 emu, the retentivity (M_r) was 39.584×10^{-3} emu and the coercivity value (H_c) was 139.61 Oe. On the other hand, for $ZnFe_2O_4$ sample with Cu^{2+} ions, the saturation magnetization (M_s) retentivity (M_r) and the coercivity value (H_c) were found to be 0.21271 emu, 71.022×10^{-3} emu and 285.91 Oe, respectively.

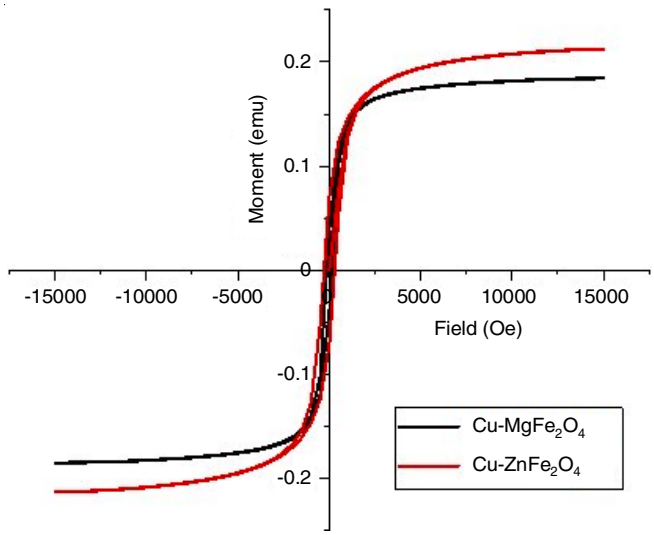

Fig. 4. VSM curves of Cu-$MgFe_2O_4$ and Cu-$ZnFe_2O_4$ nanoferrites

An increase in saturation magnetization for both samples indicates that the addition of Cu^{2+} ions has increased the magnetic moment of the nanoferrites. The increase in coercivity value for the $ZnFe_2O_4$ sample with Cu^{2+} ions indicates that the sample

has become more resistant to demagnetization, which is a desirable property for several applications, such as magnetic data storage. The increase in retentivity for the $ZnFe_2O_4$ sample with Cu^{2+} ions also indicates that the sample can maintain its magnetization in the absence of an external magnetic field. Overall, these results demonstrate the effectiveness of the sol-gel method in synthesizing Cu^{2+} doped $MgFe_2O_4$ and $ZnFe_2O_4$ nanoferrites with enhanced magnetic properties.

Applications: The impact and comparison of the prepared copper doped metal nanoferrites on pollutant removal from the locally collected pharmaceutical wastewater using the membrane bioreactor (MBR) system are shown in Table-1.

TABLE-1
EFFECT OF NANOFERRITES REMOVAL OF POLLUTANTS FROM PHARMACEUTICAL WASTEWATER

Parameter(s)	Raw water	Cu-$MgFe_2O_4$	Cu-$ZnFe_2O_4$	General standard for Discharge of environmental pollutants Part-A effluents (Schedule-VI) standard limits	
				Inland surface water	Public sewers
pH @ 25 °C	7.36	7.12	6.24	5.5-9.0	5.5-9.0
Colour (Hazen)	140	160	155	300	–
Turbidity (NTU)	6.4	6.8	6.6	–	–
Temperature (°C)	25.0	25.0	25.0	Shall not exceed 5 °C above the receiving water temperature	
Oil & grease (mg/L)	12.4	10.2	10.4	10	20
Total residual chlorine	3.2	2.6	2.2	1.0	–
Odour (Qualitative)	Pungent	Pungent	Pungent	–	–
Suspended solids (mg/L)	134.6	136.2	130.6	100	600
Ammoniacal nitrogen as (NH_3-N) (mg/L)	76.2	74.6	72.4	50	50
Total Kjeldahl nitrogen (TKN) as N (mg/L)	138.6	134.2	130.6	100	–
Free ammonia (as NH_3-N) (mg/L)	18.2	17.8	16.4	5.0	–
BOD (3 days @ 27 °C) (mg/L)	216	196	188	30	350
COD (mg/L)	2112	1920	1852	250	–
Total arsenic (mg/L)	0.16	0.12	0.10	0.2	0.2
Mercury (mg/L)	< 0.01	< 0.01	< 0.01	0.01	0.01
Lead (mg/L)	0.06	0.04	0.04	0.1	1.0
Cadmium (mg/L)	< 0.005	< 0.005	< 0.005	2.0	1.0
Hexavalent chromium (mg/L)	1.32	1.12	1.08	0.1	2.0
Total chromium (mg/L)	2.64	2.14	2.10	2.0	2.0
Copper (mg/L)	0.42	0.38	0.32	3.0	3.0
Zinc (mg/L)	12.26	10.72	10.26	5.0	15.0
Selenium (mg/L)	0.06	0.04	0.04	0.05	0.05
Nickel (mg/L)	2.78	2.64	2.42	3.0	3.0
Cyanide (mg/L)	0.12	0.08	0.06	0.2	2.0
Fluoride (mg/L)	4.34	4.12	3.96	2.0	15.0
Dissolved phosphates (mg/L)	7.26	7.04	6.74	5.0	–
Sulphide (mg/L)	0.62	0.58	0.52	2.0	–
Phenolic compounds (C_6H_5OH) (mg/L)	3.6	3.2	2.8	1.0	5.0
Radioactive materials					
Alpha emitters micro curie (mg/L)	6×10^{-6}	5×10^{-6}	4×10^{-6}	10^{-7}	10^{-7}
Beta emitters micro curie (mg/L)	3×10^{-5}	3×10^{-5}	2×10^{-5}	10^{-6}	10^{-6}
Bio-assay test	0% Survival of fish after 96 h	0% Survival of fish after 96 h	0% Survival of fish after 96 h	Minimum 90% Survival of fish after 96 h with 90% effluent and 10% dilution water	
Manganese (mg/L)	0.012	0.010	0.008	2.0	2.0
Iron (mg/L)	3.34	3.12	3.04	3.0	3.0
Vanadium (mg/L)	< 0.05	< 0.05	< 0.05	0.2	0.2
Nitrate (mg/L)	42.4	38.6	36.4	10	–
Total hardness ($CaCO_3$) (mg/L)	464	430	404	–	–
Calcium (mg/L)	116	106	102	–	–
Magnesium (mg/L)	42	40	36	–	–
Total alkalinity ($CaCO_3$) (mg/L)	564	512	492	–	–
Chlorides (mg/L)	420	378	350	600	–
Total dissolved solids (mg/L)	1924	1512	1394	1500	–
Sulphate (mg/L)	316	254	216	400	–
Dissolved oxygen (mg/L)	1.8	2.6	2.8	4.0	–
Pesticides (µg/L)	36.4	24.8	22.6	–	–
Pigment content (mg/L)	5.2	4.6	4.2	–	–
Dye content (mg/L)	2.8	2.2	2.2	–	–

Note: BOD-Biochemical oxygen demand, COD-Chemical oxygen demand, Hyphen (–) denotes limits not provided by PCB. As per the above analyzed Schedule-VI discharge standard parameters for Inland surface water quality was deviated from the standards, so this water is contaminated and polluted due to the interference of the nearest domestic/commercial/industrial effluents and wastewater.

The pH levels at 25 ºC for the different samples are within the acceptable range of 5.5 to 9.0. The untreated water exhibits a pH of 7.36, whereas the treated Cu-$MgFe_2O_4$ displays a pH of 7.12 and Cu-$ZnFe_2O_4$ shows a pH of 6.24. In terms of colour, measured in Hazen units, the raw water sample has a colour intensity of 140, whereas Cu-$MgFe_2O_4$ and Cu-$ZnFe_2O_4$ have the colour intensity of 160 and 155, respectively. While the limit for colour in inland surface water is 300, there is no specified standard limit for public sewers. Regarding turbidity, all samples show relatively low turbidity values. The raw water sample has a turbidity of 6.4 NTU, Cu-$MgFe_2O_4$ has a turbidity of 6.8 NTU and Cu-$ZnFe_2O_4$ has a turbidity of 6.6 NTU. The limit for turbidity in inland surface water is 300 NTU, but there is no specified standard limit for public sewers. In terms of oil and grease content, the raw water sample has a concentration of 12.4 mg/L, while Cu-$MgFe_2O_4$ and Cu-$ZnFe_2O_4$ have concentrations of 10.2 mg/L and 10.4 mg/L, respectively. These values exceed the standard limit for inland surface water.

The raw water sample has a residual chlorine concentration of 3.2 mg/L, while Cu-$MgFe_2O_4$ has a concentration of 2.6 mg/L and Cu-$ZnFe_2O_4$ has a concentration of 2.2 mg/L. The acceptable range for residual chlorine in both inland surface water and public sewers is not specified. The suspended solids concentration of the raw water sample was 134.6 mg/L, while Cu-doped $MgFe_2O_4$ and $ZnFe_2O_4$ were 136.2 and 130.6 mg/L, respectively. The raw water sample has an ammonical nitrogen concentration of 76.2 mg/L, Cu-$MgFe_2O_4$ and Cu-$ZnFe_2O_4$ has 74.6 mg/L and 72.4 mg/L, respectively. The raw water sample exhibits a TKN content of 138.6 mg/L, while Cu-$MgFe_2O_4$ and Cu-$ZnFe_2O_4$ has a concentration of 134.2 and 130.6 mg/L, respectively. The established threshold for total Kjeldahl nitrogen (TKN) in inland surface water was 100 mg/L, however the level for public sewers remains unspecified.

Similarly, both the Cu-$MgFe_2O_4$ and Cu-$ZnFe_2O_4$ nanoferrites have succesfully reduced the other waterwater parameters like BOD, COD, heavy as well as toxic metals/organic compounds too. However, there are still challenges in removing Cr(IV) and phenolic compounds, as their concentrations exceed the limits for inland surface water. The concentrations of copper, zinc, selenium, nickel, cyanide, and dissolved phosphates remain within the standard limits. The MBR system with nanoferrites also helps in reducing fluoride, sulphide and radioactivity levels below the specified standards. Overall, the nanoferrites contribute to the effective removal of pollutants, but further optimization may be required to ensure compliance with all water quality standards.

Conclusion

In conclusion, the synthesis of copper-doped magnesium nanoferrite and zinc nanoferrite nanoparticles using the sol-gel method was successfully conducted. The characterization confirmed the formation of the spinel structure of the nanoferrites. The UV spectra showed a characteristic peaks at 286 nm for copper doped magnesium nanoferrite and at 279 nm for copper doped zinc nanoferrite. The FTIR spectra confirm the formation of Cu-doped $MgFe_2O_4$ and Cu-doped $ZnFe_2O_4$ nanoferrites. The addition of Cu^{2+} ions has a significant impact on the magnetic properties of the nanoferrites, as evidenced by the increase in the saturation magnetization and coercivity values for both copper-doped metal nanoferrites. The use of prepared copper doped metal nanoferrites in the membrane bioreactor system for treating pharmaceutical wastewater shows promising results in removing various pollutants. The nanoferrites effectively reduce concentrations of heavy metals such as lead and cadmium, which fall within the acceptable range for both inland surface water and public sewers.

ACKNOWLEDGEMENTS

The authors are grateful to The Head, Chemistry Research Laboratory, Bhavan's Hazarimal Somani College, Mumbai, India for providing the basic research facilities. Thanks are also due to The Director, Institute of Science, Mumbai, India for providing the antifungal activity.

CONFLICT OF INTEREST

The authors declare that there is no conflict of interests regarding the publication of this article.

REFERENCES

1. K.K. Kadyrzhanov, K. Egizbek, A.L. Kozlovskiy and M.V. Zdorovets, *Nanomaterials*, **9**, 1079 (2019); https://doi.org/10.3390/nano9081079
2. T. Dippong, E.A. Levei and O. Cadar, *Nanomaterials*, **11**, 1560 (2021); https://doi.org/10.3390/nano11061560
3. M.S. Chavali and M.P. Nikolova, *SN Appl. Sci.*, **1**, 607 (2019); https://doi.org/10.1007/s42452-019-0592-3
4. A. Ali, T. Shah, R. Ullah, P. Zhou, M. Guo, M. Ovais, Z. Tan and Y. Rui, *Front Chem.*, **9**, 629054 (2021); https://doi.org/10.3389/fchem.2021.629054
5. I. Khan, K. Saeed and I. Khan, *Arab. J. Chem.*, **12**, 908 (2019); https://doi.org/10.1016/j.arabjc.2017.05.011
6. S.K. Murthy, *Int. J. Nanomedicine*, **2**, 129 (2007).
7. N. Joudeh and D. Linke, *J. Nanobiotechnol.*, **20**, 262 (2022); https://doi.org/10.1186/s12951-022-01477-8
8. S. Sim and N.K. Wong, *Biomed. Rep.*, **14**, 42 (2021); https://doi.org/10.3892/br.2021.1418
9. G. Xian, S. Kong, Q. Li, G. Zhang, N. Zhou, H. Du and L. Niu, *Front. Chem.*, **8**, 177 (2020); https://doi.org/10.3389/fchem.2020.00177
10. M.A. Rafiq, A. Javed, M.N. Rasul, M.A. Khan and A. Hussain, *Ceram. Int.*, **46**, 4976 (2020); https://doi.org/10.1016/j.ceramint.2019.10.237
11. M.I. Abdel Maksoud, R.A. Fahim, A.E. Shalan, M. Abd Elkodous, S.O. Olojede, A.I. Osman, C. Farrell, A.A. Al-Muhtaseb, A.S. Awed, A.H. Ashour and D.W. Rooney, *Environ. Chem. Lett.*, **19**, 375 (2021); https://doi.org/10.1007/s10311-020-01075-w
12. L.A. Achola, S. Shubhashish, Z. Tobin, Y. Su, L.F. Posada, Y. Dang, J. Shi, A.G. Meguerdichian, M. Jain and S.L. Suib, *Chem. Mater.*, **34**, 7692 (2022); https://doi.org/10.1021/acs.chemmater.2c00684
13. M. Amiri, M. Salavati-Niasari and A. Akbari, *Adv. Colloid Interface Sci.*, **265**, 29 (2019); https://doi.org/10.1016/j.cis.2019.01.003
14. L.A. Kafshgari, M. Ghorbani and A. Azizi, *Particul. Sci. Technol.*, **37**, 900 (2018); https://doi.org/10.1080/02726351.2018.1461154
15. N. Gupta, P. Jain, R. Rana and S. Shrivastava, *Mater. Today Proc.*, **4**, 342 (2017); https://doi.org/10.1016/j.matpr.2017.01.031
16. P.K. Roy and J. Bera, *J. Mater. Process. Technol.*, **197**, 279 (2008); https://doi.org/10.1016/j.jmatprotec.2007.06.027

17. N.A. Tien, V.O. Mittova, B.V. Sladkopevtsev, V.Q. Mai, I.Y. Mittova and B.X. Vuong, *Solid State Sci.*, **138**, 107149 (2023); https://doi.org/10.1016/j.solidstatesciences.2023.107149
18. R. Strobel and S.E. Pratsinis, *J. Mater. Chem.*, **17**, 4743 (2007); https://doi.org/10.1039/b711652g
19. I.P. Parkin, G. Elwin, M.V. Kuznetsov, Q.A. Pankhurst, Q.T. Bui, G.D. Forster, L.F. Barquín, A.V. Komarov and Y.G. Morozov, *J. Mater. Process. Technol.*, **110**, 239 (2001); https://doi.org/10.1016/S0924-0136(00)00889-X
20. T. Adschiri, Y. Hakuta and K. Arai, *Ind. Eng. Chem. Res.*, **39**, 4901 (2000); https://doi.org/10.1021/ie0003279
21. D. Segal, Chemical Synthesis of Advanced Ceramic Materials, Cambridge University Press (1991).
22. S.N. Pund, P.A. Nagwade, A.V. Nagawade, S.R. Thopate and A.V. Bagade, *Mater. Today Proc.*, **60**, 2194 (2022); https://doi.org/10.1016/j.matpr.2022.02.444
23. Z. Dong, W. Hu, Z. Ma, C. Li and Y. Liu, *Mater. Chem. Front.*, **3**, 1952 (2019); https://doi.org/10.1039/C9QM00422J
24. S.E. Shirsath, D. Wang, S.S. Jadhav, M.L. Mane and S. Li, Ferrites Obtained by Sol-Gel Method, In: L. Klein, M. Aparicio and A. Jitianu, Handbook of Sol-Gel Science and Technology, Springer, Cham, pp. 695-735 (2018).
25. A.V. Gongal, D.V. Nandanwar, D.S. Badwaik, S.S. Wanjari, V.S. Harode and S.M. Suryawanshi, *Nano-Struct. Nano-Objects*, **39**, 101248 (2024); https://doi.org/10.1016/j.nanoso.2024.101248
26. M.N. Kiani, M.S. Butt, I.H. Gul, M. Saleem, M. Irfan, A.H. Baluch, M.A. Akram and M.A. Raza, *ACS Omega*, **8**, 3755 (2023); https://doi.org/10.1021/acsomega.2c05226
27. T. Vigneswari and P. Raji, *J. Mol. Struct.*, **1127**, 515 (2017); https://doi.org/10.1016/j.molstruc.2016.07.116
28. D. Parajuli, N. Murali, A.V. Rao, A. Ramakrishna and K. Samatha, *S. Afr. J. Chem. Eng.*, **42**, 106 (2022); https://doi.org/10.1016/j.sajce.2022.07.009
29. S.Y. Mulushoa and N. Murali, *Inorg. Chem. Commun.*, **145**, 110033 (2022); https://doi.org/10.1016/j.inoche.2022.110033
30. F. Sharifianjazi, M. Moradi, N. Parvin, A. Nemati, A.J. Rad, N. Sheysi, A. Abouchenari, A. Mohammadi, S. Karbasi, A. Esmaeilkhanian, M. Irani, Z. Ahmadi, A. Pakseresht, S. Sahmani and M. Shahedi Asl, *Ceram. Int.*, **46**, 18391 (2020); https://doi.org/10.1016/j.ceramint.2020.04.202
31. B. Mishra, B. Munisha, J. Nanda, K.J. Sankaran and S. Suman, *Mater. Chem. Phys.*, **292**, 126791 (2022); https://doi.org/10.1016/j.matchemphys.2022.126791
32. S.F. Mansour, S. Wageh, R. Al-Wafi and M.A. Abdo, *J. Alloys Compd.*, **856**, 157437 (2021); https://doi.org/10.1016/j.jallcom.2020.157437
33. P. Thakur, S. Taneja, D. Chahar, B. Ravelo and A. Thakur, *J. Magn. Magn. Mater.*, **530**, 167925 (2021); https://doi.org/10.1016/j.jmmm.2021.167925
34. M.A. Rafiq, M.A. Khan, M. Asghar, S.Z. Ilyas, I. Shakir, M. Shahid and M.F. Warsi, *Ceram. Int.*, **41**, 10501 (2015); https://doi.org/10.1016/j.ceramint.2015.04.141
35. S. Perveen, S. Hafeez, S. Rashid, S.U. Asad, M.Z. Khan and F. Azad, *Mater. Chem. Phys.*, **297**, 127303 (2023); https://doi.org/10.1016/j.matchemphys.2023.127303
36. B. Issa, I.M. Obaidat, B.A. Albiss and Y. Haik, *Int. J. Mol. Sci.*, **14**, 21266 (2013); https://doi.org/10.3390/ijms141121266
37. A. Soufi, H. Hajjaoui, R. Elmoubarki, M. Abdennouri, S. Qourzal and N. Barka, *Appl. Surface Sci. Adv.*, **6**, 100145 (2021); https://doi.org/10.1016/j.apsadv.2021.100145
38. C.A. Charitidis, P. Georgiou, M.A. Koklioti, A.-F. Trompeta and V. Markakis, *Manufacturing Rev.*, **1**, 11 (2014); https://doi.org/10.1051/mfreview/2014009